# Constructing the Residual Circulation of the ACC from Observations

RICHARD H. KARSTEN

*Department of Mathematics and Statistics, Acadia University, Wolfville, Nova Scotia, Canada*

JOHN MARSHALL

*Department of Earth, Atmospheric and Planetary Sciences, Massachusetts Institute of Technology, Cambridge, Massachusetts*

(Manuscript received 3 August 2001, in final form 12 March 2002)

ABSTRACT

The dynamics of the meridional overturning of the Antarctic Circumpolar Current (ACC) are best described in terms of a residual circulation that sums the transport of the wind-driven Ekman layer to the transport associated with eddies. Here an attempt is made to infer the residual circulation from observations by combining altimetric data and gridded hydrographic data to estimate eddy fluxes and winds to estimate Ekman transport. At the surface, a flow directed equatorward on the poleward flank of the ACC, and directed poleward on the equatorward flank of the ACC, is deduced. This convergence of flow into the axis of the ACC drives the subduction of the Antarctic Intermediate Water. Weak southward residual flow on the equatorward boundary of the ACC indicates that here Ekman transport is offset by eddy fluxes. The sense of the deduced residual circulation suggests that buoyancy is gained by the ocean through air–sea flux poleward of the ACC, in broad agreement with observations. The surface residual circulation is mapped down to depth to yield two counterrotating meridional cells associated with the transformation of North Atlantic Deep Water and Subantarctic Mode Water into Antarctic Intermediate Water. The circulation suggested by these cells agrees remarkably well with the subsurface distribution of salinity and dissolved oxygen. The dependence of the residual circulation estimate on the magnitude of assumed eddy transfer and mixing coefficients is discussed.

## 1. Introduction

The Antarctic Circumpolar Current (ACC) dominates the dynamics of the Southern Ocean connecting the ocean basins but also isolating the seas surrounding Antarctica from the rest of the World Ocean [see the reviews of Nowlin and Klink (1986) and Rintoul et al. (2001)]. In the steady state, meridional transport of quantities across the ACC by mean and eddy processes must balance differential forcing at the surface. In this observational study we use residual-mean theory to guide an estimate of the strength and pattern of the meridional circulation of the ACC based on observations of the wind field, altimetric observations of sea surface height variability, and in situ gridded hydrographic data.

The dominant forcing of the ACC are the strong westerly winds that blow over it, imparting eastward momentum to the ocean. At the same time, due to the Coriolis force, the wind drives an overturning cell directed equatorward at the surface—the Deacon cell—carrying heat equatorward. Thus to maintain the observed mean current and stratification, there must be a balancing eastward momentum sink and a poleward transfer of heat. It is believed that eddy transfer due to instabilities of the ACC provide the balancing fluxes of heat and momentum.

Altimetric snapshots of the ACC reveal a highly unstable current with large baroclinic eddies and meanders, which feed off the potential energy stored in the sloping isopycnals of the ACC. De Szoeke and Levine (1981) argue that eddies must be largely responsible for poleward heat transport across the current. Mooring and altimetric measurements indeed suggest that there is a substantial southward heat flux associated with these eddies (Keffer and Holloway 1988; Johnson and Bryden 1989; Stammer 1998; Phillips and Rintoul 2000). Similarly, in numerical simulations advection due to eddies offsets the mean advection resulting in the ''vanishing of the Deacon cell'' (Döös and Webb 1994; Danabasoglu et al. 1994). This poleward heat flux can be directly related to a downward momentum flux through interfacial drag (Johnson and Bryden 1989; Olbers 1998). This drag allows momentum imparted at the surface to be transferred to depth where it can be dissipated by mountain drag as the ACC flows over high topographic ridges, as first suggested by Munk and Palmén (1951). Such a momentum balance has also been established in

*Corresponding author address:* Richard H. Karsten, Department of Mathematics and Statistics, Acadia University, Wolfville, NS B4P 2R6, Canada.
E-mail: richard.karsten@acadiau.ca

both observations (Phillips and Rintoul 2000) and numerical models (Ivchenko et al. 1996; Gille 1997; Olbers and Ivchenko 2001). Thus, both effects of wind forcing—meridional heat transport by the Ekman-driven flow and the momentum imparted by the wind—appear to be largely balanced by eddy fluxes.

The atmosphere also forces the ACC through surface buoyancy fluxes. Heat loss and gain at the surface change the heat content of the ocean. In addition, the Southern Ocean is a region of strong surface salinity fluxes associated with evaporation, precipitation, and ice formation and melt. Air–sea buoyancy fluxes play an essential role in the transformation of water masses (Deacon 1984; Speer et al. 2000; Karsten et al. 2002, hereafter KJM). It is in the ACC that North Atlantic Deep Water (NADW), formed in the polar North Atlantic, is transformed into Antarctic Intermediate Water (AAIW), a vital limb of the thermohaline overturning (see, e.g., Toggweiler and Samuels 1998).

Recent studies have focused on the combined effect of wind and thermohaline forcing (Marshall 1997; Gnanadesikan and Hallberg 2000; Speer et al. 2000; Marshall et al. 2002; KJM). In KJM we examined the dynamical balance of the ACC using idealized numerical experiments. We were able to generate a statistically steady circumpolar current in which forcing by the prescribed winds and surface fluxes was balanced by the transport associated with a vigorous baroclinic eddy field. Following Andrews and McIntyre (1976) and Marshall (1997) we applied residual mean theory to develop a dynamical framework whose focus was the residual circulation—the sum of the mean Eulerian flow and the transport associated with eddies (see section 3.)

In this paper we attempt to examine the residual circulation of the ACC using observations. Our goal is twofold. First, we study the balance between eddy and wind-driven circulation. Second, we estimate the residual circulation and rationalize it in terms of surface buoyancy fluxes and tracer distributions. Accomplishing these tasks requires knowledge of the eddy buoyancy fluxes. Following Holloway (1986), Keffer and Holloway (1988), and Kushner and Held (1998), we assume the eddy diffusivity is proportional to the altimetric height variance and use altimetric measurements from TOPEX/Posiedon to estimate a near-surface eddy diffusivity.

The paper is set out as follows: in section 2 we describe the wind, altimetric, and in situ gridded hydrographic observations that will be used in the study. In section 3, we review key aspects of residual-mean theory and present the inferred residual flow deduced from observations. In section 4, we discuss the results and conclude.

## 2. Observed structure of the ACC

### a. Streamlines

We calculate the surface geostrophic streamlines $\Psi_g$ using the mean sea surface height (SSH) calculated from TOPEX/Poseidon altimetry data over the period October 1992–February 1995 (obtained from the University of Texas Center for Space Research Web site: ftp.csr.utexas.edu). The streamfunction is given by

$$\Psi_g = \frac{gh}{f}, \tag{1}$$

where $g$ is the gravitational acceleration, $f$ is the Coriolis parameter, and $h$ is the mean SSH. Contours of streamlines are shown in Fig. 1. We have chosen to set the zero contour to be coincident with the axis of the ACC; positive streamlines lie poleward and negative streamlines equatorward. The contours that bound circumpolar flow (solid bold contours) correspond to streamline heights of $\Psi_g = -2.4 \times 10^4$ and $\Psi_g = 2.4 \times 10^4$, respectively. These two contours will be used to delineate the latitudinal extent of circumpolar flow on subsequent plots. Typical mean surface currents are 8 cm $s^{-1}$—$\Psi_g$ varies by $4.8 \times 10^4$ $m^2$ $s^{-1}$ over the ACC which has a mean width of 600 km.

The ACC does not follow lines of constant latitude, but, after passing through Drake Passage (60°W), jogs equatorward and progresses eastward around 50°S. It then slowly drifts poleward until it again reaches Drake Passage at roughly 60°S. The path shows the influence of topography and is, in general, steered northward after it passes over high ridges, in rough agreement with the theory of mountain drag (see Johnson and Bryden 1989). More detailed discussions of how topography affects the path can be found in, for example, Marshall (1995), Orsi et al. (1995), and Moore et al. (1999).

The streamlines shown in Fig. 1 are used to compute streamwise averages. Although mean streamlines based on altimetry contain errors associated with uncertainty in the geoid, they do not compromise the calculations presented here because they are only used to define the path along which ''zonal'' averages are taken. We adopt a streamline coordinate system with $x$ being the eastward alongstreamline coordinate and $y$ the equatorward cross-streamline coordinate, respectively. The corresponding alongstreamline and cross-streamline velocities are $u$ and $v$. Mean values are defined as along-streamline averages and our focus will be determining cross-stream transports. For simplicity our notation is in Cartesian coordinates although spherical coordinates are used in all calculations.

### b. Hydrography

In keeping with the analysis of KJM, we will discuss the budgets of the ACC in terms of buoyancy. Starting from Levitus and Boyer (1994) annual mean data for the potential temperature and salinity we calculate the potential density $\sigma$ using the nonlinear equation of state (Gill 1982); the buoyancy is defined by $b = -g\sigma/\rho_0$, where $\rho_0 = 1030$ kg $m^{-3}$ is the average density of seawater. (The mean isopycnals can be seen later in Fig. 4.) It should be noted that almost all isopycnals outcrop

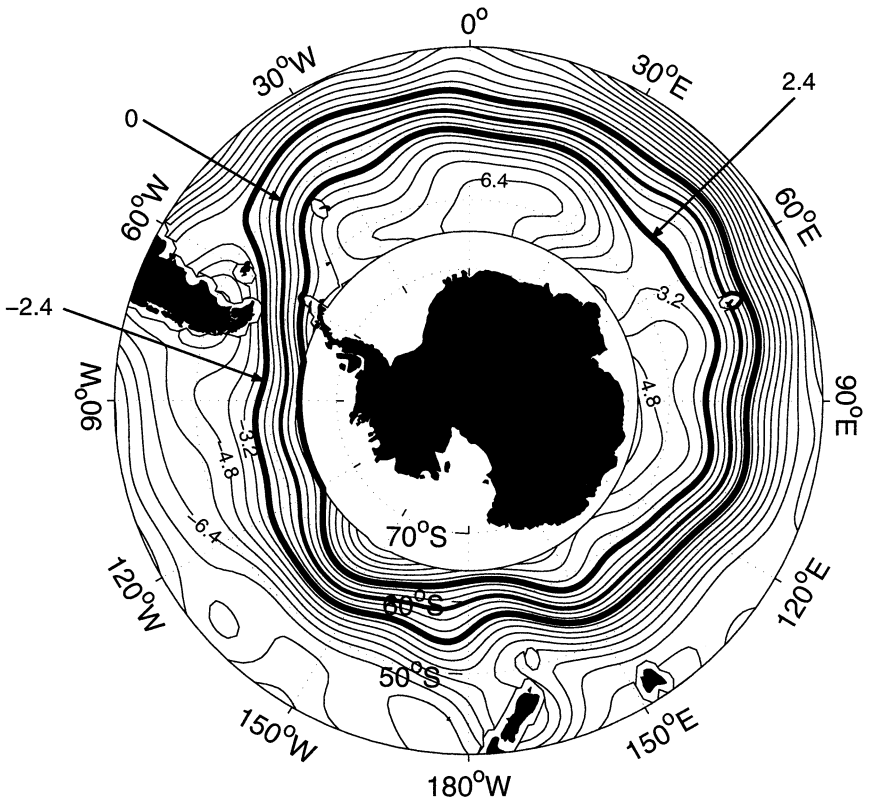


FIG. 1. The geostrophic streamlines $\Psi g$ as given by (1). The contour interval is $0.8 \times 10^4$ m$^2$ s$^{-1}$ with the value increasing as one travels poleward and the zero contour located at the axis of the ACC. The bold solid lines mark the boundaries of circumpolar flow: $\Psi g = \pm 2.4 \times 10^4$ m$^2$ s$^{-1}$.

and therefore ''feel'' surface fluxes. In our calculations we also make use of a mixed layer buoyancy, $b_m$, computed by averaging the buoyancy over the annual-mean mixed layer depth, $h_m$, as given by Levitus and Boyer (1994).

### c. Wind forcing

The ACC is forced by strong westerly winds that impart eastward momentum at the surface. Since the ACC has an equivalent barotropic structure (see Killworth 1992; Marshall et al. 1993; Karsten and Marshall 2002), it is reasonable to assume the mean geostrophic flow at all depths is captured by the streamfunction plotted in Fig. 1. The surface Ekman transport and its return flow at depth is directed across mean streamlines. Along with the surface Ekman transport there will be a vertical upwelling associated with surface divergence of this transport and a pumping associated with convergence. This wind-driven overturning circulation, known as the Deacon cell, upwells in polar regions, is directed northward at the surface, and sinks in the subtropics. This circulation is closed at depth by a return flow, the details of which are not essential for the calculation presented here. Since the surface buoyancy is much higher than the buoyancy at depth, this wind-driven cell drives a net buoyancy flux equatorwards. Hence the winds, through Ekman transport, drive a net densification of the polar regions.

The meridional circulation can be written in terms of a mean streamfunction,

$$\overline{v} = -\frac{\partial \overline{\Psi}}{\partial z}, \qquad \overline{\omega} = \frac{\partial \overline{\Psi}}{\partial y},$$

with $\overline{\Psi}$ given by the Ekman transport,

$$\overline{\Psi} = -\frac{\overline{\tau}}{\rho_0 f}, \tag{2}$$

where $\overline{\tau}$ is the time-averaged wind stress integrated along the mean streamlines. Knowledge of the detailed structure of the flow in the Ekman layer is not required here, but we note that $\overline{w}$ must vanish at the surface and so $\overline{\Psi} = 0$ there: the Ekman value is achieved, we assume, at the base of the Ekman layer.

To map the Ekman transport we use the wind stress from the Southampton Oceanography Centre (see Josey et al. 1998), hereafter SOC winds. These wind stress data are roughly 30% higher at the poleward boundary of the ACC than, for example, the Hellerman and Rosenstein (1983) data, hereafter HR winds, and are thought to be a better representation of Southern Hemi-

sphere winds (for comparison, in many figures we include the results of calculations using both sets of wind data). We obtain a net transport by integrating (2) along the streamlines shown in Fig. 1. The result is a net equatorward transport in excess of 20 Sv (Sv $\equiv 10^6$ m$^3$ s$^{-1}$) throughout the extent of the ACC as can be seen later in Fig. 3.

### d. Eddy variability

The ACC is a highly variable region with the large store of potential energy inherent in the sloping isopycnals being released through vigorous baroclinic instability leading to large meanders and eddies. These eddies result in a downgradient flux of heat as they sweep warm waters to the south and cold waters to the north. Unfortunately, detailed mooring measurements that allow calculation of this eddy flux are few and far between. Moreover, due to the presence of large rotational eddy fluxes, particularly in the near surface layers—see Marshall and Shutts (1981)—they are very difficult to interpret dynamically. Johnson and Bryden (1989) found a strong poleward flux of heat in Drake Passage, but Bryden and Heath (1985) did not find a statistically significant heat flux using data from a mooring southeast of New Zealand. Recently, Phillips and Rintoul (2000) examined mooring data south of Australia and found a strong poleward heat flux that was statistically significant, but only when calculated with reference to a ''shear'' coordinate system which varied with the flow. It appears that the large meanders of the ACC vary on such slow time scales that a statistically significant calculation of their fluxes require a time series longer than those obtained from moorings. Even when the mooring data do suggest a significant poleward eddy heat flux, these data have limited spatial and temporal coverage. In order to estimate eddy fluxes on a global scale we therefore attempt to make use of altimetric data.

Estimates of eddy fluxes can be made if the flux is assumed to be directed down the large-scale gradient, that is,

$$\overline{v'b'} = -K\frac{\partial \overline{b}}{\partial y}, \tag{3}$$

and we have estimates of the eddy diffusivity $K$ and the mean buoyancy $\overline{b}$. Holloway (1986) and Keffer and Holloway (1988) assumed that $K$ is proportional to the root mean square of the geostrophic streamfunction variability; that is,

$$K = \alpha(\overline{\Psi_g'^2})^{1/2} = \alpha\frac{g}{|f|}(\overline{h'^2})^{1/2}, \tag{4}$$

where $\Psi_g'$ is the variability in the streamfunction, $h'$ is the corresponding sea surface height variability, and $\alpha$ is a constant of proportionality. Kushner and Held (1998) have tested the approach with atmospheric data and found that it captured the spatial variation of the diffusivity with optimum values of $\alpha$ varying between 0.2 and 0.4. In the appendix, we have also tested the method using the numerical simulations presented in KJM. We find that (4) is a good predictor of the eddy diffusivities when $\alpha = 0.26$. It should be noted that (4) gives an estimate of the surface diffusivity only and says nothing of how this diffusivity will vary with depth. Fortunately our method only requires knowledge of surface diffusivities.

In Fig. 2a, we plot $K$ using (4) with $\overline{h'^2}^{1/2}$ obtained from TOPEX/Poseidon sea surface height during October 1992–February 1995 (the data are available online at ingrid.mit.edu) and assuming that $\alpha = 0.26$. The figure highlights regions of moderate eddy activity $2500 > K > 1500$ m$^2$ s$^{-1}$ and strong eddy activity $K > 2500$ m$^2$ s$^{-1}$. The ACC, especially its equatorward flank, is a relatively active region with several hot spots of high eddy activity lying downstream of large topographic features.

The streamwise average of the diffusivity is plotted in Fig. 2b. We see that the diffusivity increases from 1700 m$^2$ s$^{-1}$ at the southern boundary of the ACC to 2500 m$^2$ s$^{-1}$ at the northern boundary with a mean value of roughly 2100 m$^2$ s$^{-1}$. The error bars assume a 1-cm error in the altimetric value of $\overline{h'^2}^{1/2}$ and a 10% error in the value of $\alpha$.

These estimates of diffusivity are higher than those of Stammer (1998) who inferred $K$ from local Eady growth rates using hydrographic data following the ideas set out in Visbeck et al. (1997). It is also larger than the canonical 1000 m$^2$ s$^{-1}$ used in course-resolution numerical models and analytical theories (Marshall 1997; Gnanadesikan 1999; Marsh et al. 2000; Gent et al. 2001). Stammer (1998) argues that the Holloway method overestimates the diffusivity by a factor of 2 since 50% of sea surface height variability is at large spatial scales and thus unrelated to eddy transfer processes. Note, however, that our estimates based on (4) is of a *surface* diffusivity whereas the methods of obtaining $K$ discussed in Visbeck et al. (1997) are appropriate to interior values of $K$. Numerical models (e.g., see KJM) suggest that the eddy diffusivity tends to increase as the surface is approached. Thus we adopt a value $\alpha = 0.26$, yielding a $K$ at the upper end of the canonical range which we believe to be appropriate for this, the most energetic region of the ocean. We discuss the sensitivity of our results to this choice in section 3e.

## 3. Residual circulation

### a. Dynamical background

In this section we briefly review residual-mean theory as applied to the ACC (see KJM for more details). We begin with the time- and along-stream-averaged equations in the statistically steady state. For incompressible flow, conservation of buoyancy can be written as

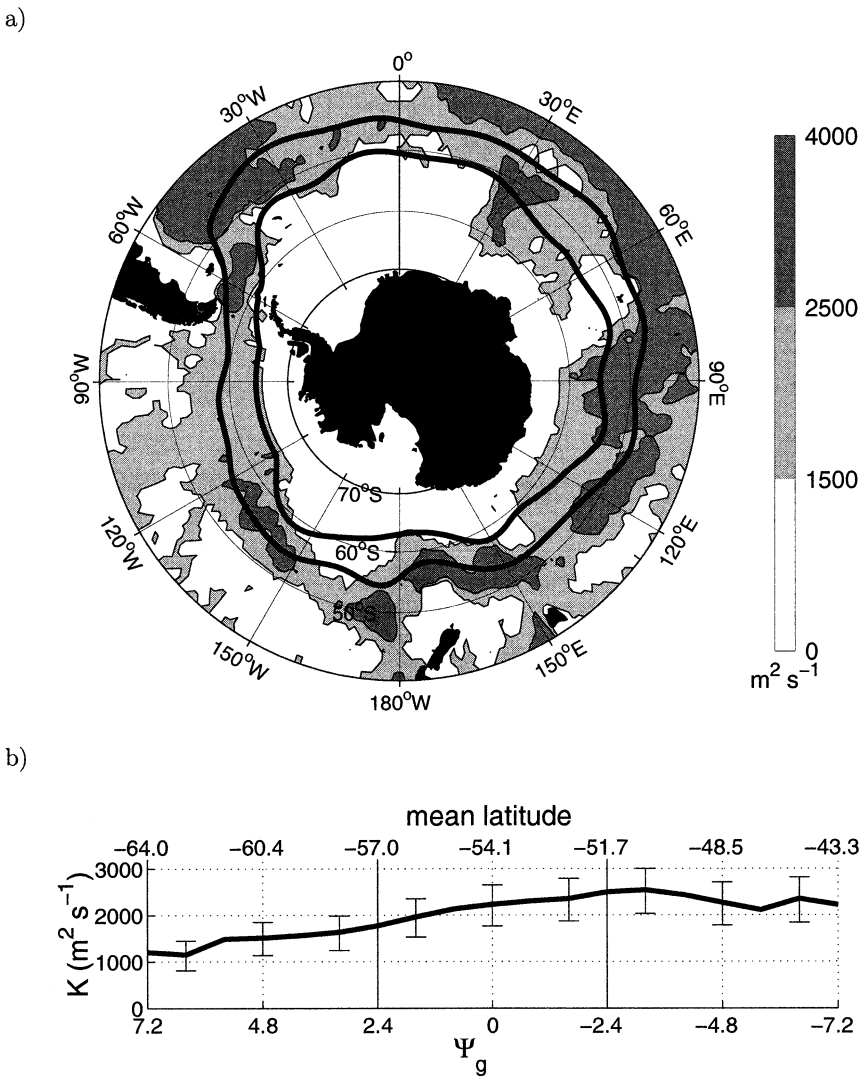


FIG. 2. (a) The eddy diffusivity $K$ calculated using the formula (4) with $\alpha = 0.26$ and $\overline{h'^2}$ from altimetry and (b) the streamwise average of the diffusivity with errors bars as discussed in the text.

$$\overline{v}\frac{\partial \overline{b}}{\partial y} + \overline{w}\frac{\partial \overline{b}}{\partial z} + \frac{\partial}{\partial y}(\overline{v'b'}) + \frac{\partial}{\partial z}(\overline{w'b'}) = \frac{\partial B}{\partial z} + \kappa\frac{\partial^2 \overline{b}}{\partial z^2}, \quad (5)$$

where $y$ ($v$) and $z$ ($w$) are the cross-stream and vertical coordinate (velocity), respectively. In (5) the variables have been separated into mean (along-stream and time) quantities, $\overline{b}$, and the perturbations about this mean, $b'$. The buoyancy forcing has been written as the divergence of a buoyancy flux, $B$, with the flux taken as positive if it is directed into the ocean. Small-scale mixing is represented by a diffusive process acting vertically at rate $\kappa$.

It is very instructive to rewrite (5) in terms of a residual-mean meridional circulation [see Andrews et al. (1987) or KJM for further discussion]. We derive the residual mean circulation by interpreting the divergence of the eddy fluxes as an advective process, thus

$$\frac{\partial}{\partial y}(\overline{v'b'}) + \frac{\partial}{\partial z}(\overline{w'b'}) = \overline{v}^*\frac{\partial \overline{b}}{\partial y} + \overline{w}^*\frac{\partial \overline{b}}{\partial z} + \text{diapycnal eddy transport}, \quad (6)$$

where the residual velocities, $\overline{v}^*$ and $\overline{w}^*$, are determined by

$$\Psi^* = -\frac{\overline{w'b'}}{\overline{b}_y}, \quad (7)$$

the ''bolus'' transport streamfunction (using the definition favored by Held and Schneider 1999), and at the sea surface $w^*$ and hence $\Psi^* = 0$.

Using (6) and assuming that the eddy transport ($\overline{v'b'}$, $\overline{w'b'}$) is directed along $\overline{b}$ surfaces so that the diapycnal term vanishes in (5)—the limit of ''adiabatic eddies''—we can rewrite (5) in the transformed Eulerian mean (TEM) form:

$$J(\Psi_{\text{res}}, \overline{b}) = \frac{\partial B}{\partial z} + \kappa \frac{\partial^2 \overline{b}}{\partial z^2}, \tag{8}$$

where $J(A, C) = A_y C_z - A_z C_y$, and we have introduced the residual streamfunction $\Psi_{\text{res}}$ defined thus

$$\Psi_{\text{res}} = \overline{\Psi} + \Psi^*, \tag{9}$$

with the associated residual velocities:

$$\overline{v}_{\text{res}} = -\frac{\partial \Psi_{\text{res}}}{\partial z} = \overline{v} + v^*, \quad \overline{w}_{\text{res}} = \frac{\partial \Psi_{\text{res}}}{\partial y} = \overline{w} + w^*.$$

Equation (8) states that the advection of buoyancy by the residual circulation balances surface buoyancy forcing and small-scale diffusion.

If we integrate (8) over the depth of the mixed layer $h_m$, where vertical gradients of buoyancy vanish, then we have

$$\Psi_{\text{res}}(z = -h_m)\frac{\partial \overline{b}_m}{\partial y} = B_s - \kappa \frac{\partial \overline{b}}{\partial z}(z = -h_m), \tag{10}$$

where $\overline{b}_m(y)$ is the mixed layer buoyancy and $\Psi_{\text{res}} = 0$ at the surface because $\overline{w} = w^* = 0$ there. Equation (10) can also be obtained by considering the budget of buoyancy between two $\overline{b}$ surfaces following Marshall (1997). If the vertical diffusion is negligibly small, then Eq. (10) states simply that the net meridional transport by the residual circulation in the mixed layer balances the surface buoyancy flux. In the Southern Ocean $\partial \overline{b}_m/\partial y > 0$. Thus, a surface gain of buoyancy by the ocean, $B_s > 0$, is associated with an equatorward surface residual velocity, $\Psi_{\text{res}} > 0$; for surface waters to move equatorward, up the buoyancy gradient, they must gain buoyancy.

The beauty of relationship (10) is that it is a purely surface balance and does not demand knowledge of the eddy fluxes at depth. The difficulty of relationship (10) is that observations of surface buoyancy flux and vertical mixing processes are very uncertain in the ACC.

We now proceed with an alternative approach to mapping out $\Psi_{\text{res}}$ by directly estimating the terms that make it up: $\overline{\Psi}$ and $\Psi^*$ in (9).

### *b. Residual circulation from observations*

#### 1) ESTIMATE OF THE NEAR-SURFACE RESIDUAL FLOW

We now attempt to construct $\Psi_{\text{res}}$ from observations by summing $\overline{\Psi}$ and $\Psi^*$. We estimate $\overline{\Psi}$ from (2) and observations of the wind stress. But what about $\Psi^*$?

We suppose that the eddy flux beneath the mixed layer is adiabatic so that

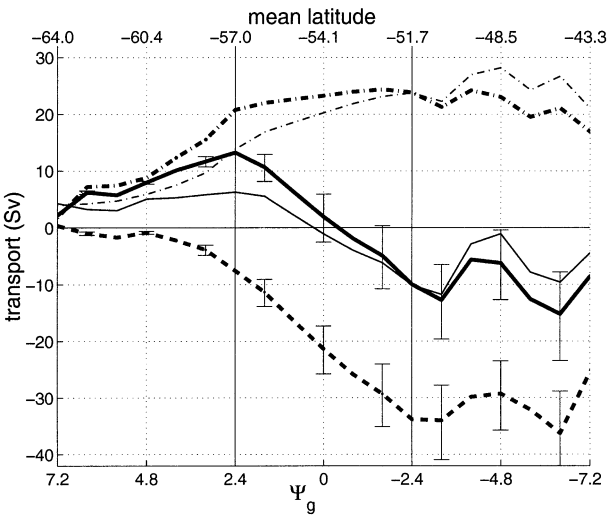


FIG. 3. The Ekman transport, $\overline{\Psi}$, given by (2): dash–dot. The eddy induced transport, $\Psi^*$, given by (11): dashed. The residual transport, $\Psi_{\text{res}}$, given by (9): solid. The thin dash–dot and solid lines are based on the HR winds; the thick dash–dot and solid lines are based on SOC winds. The error bars on the eddy-induced transport and residual circulation are calculated from the errors in the eddy diffusivity.

$$\frac{\overline{w'b'}}{\overline{v'b'}} = -\frac{\overline{b}_y}{\overline{b}_z}.$$

Then $\Psi^*$, from (7), can be written thus:

$$\Psi^* = \frac{\overline{v'b'}}{\overline{b}_z}.$$

To compute $\overline{v'b'}$ we use (3), with the eddy diffusivity evaluated as described following (4), giving

$$\Psi^* = -\alpha \frac{g}{|f|}(\overline{h'^2})^{1/2}\frac{\overline{b}_y}{\overline{b}_z}. \tag{11}$$

Finally, we use observations of $\overline{b}$ from Levitus and Boyer (1994) to evaluate $\overline{b}_y$ and $\overline{b}_z$. The results are shown in Fig. 3, where we plot $\Psi_{\text{res}}$ as well as its two components, $\overline{\Psi}$ and $\Psi^*$.

Our residual circulation estimate suggests that there is some 13.2 Sv flowing equatorward at the surface on the poleward flank of the ACC and 10 Sv flowing poleward on the equatorward flank of the ACC. Thus, within the ACC there is an implied subduction of 23.2 Sv of water—the Antarctic convergence. The point where the residual circulation vanishes near the northern ACC boundary marks the position where equatorward traveling, cold Antarctic Surface Water (AASW) meets poleward traveling, warm Subantarctic Mode Water (SAMW)—the Polar Front.

The strength of this residual circulation is similar to that suggested by Marshall (1997) but somewhat smaller than that in Speer et al. (2000) (see the discussion below). The 10 Sv of residual flow on the equatorward flank of the ACC is weak in comparison to the Ekman transport (23.8 Sv) and the eddy-induced transport (33.8

Sv). Thus, at this location, we do indeed observe a leading order balance of the winds and eddies, reminiscent of that seen in KJM. However, on the poleward flank the residual circulation (13.2 Sv) actually exceeds the eddy-induced flow (7.6 Sv) indicating that buoyancy forcing must enter the leading order dynamics here.

Our calculation does not result in a poleward surface flow poleward of the ACC that would supply deep-water formation near Antarctica (see Sloyan and Rintoul 2001). However, satellite altimetry does not allow one to examine regions south of 64.5°S, so our analysis could not discern such a flow even if it existed. Additionally, one may argue that the deep-water formation process is inherently a convective process and probably localized to the shelf. Since our arguments do not take into account convective fluxes, our derived residual circulation does not include the transport associated with them.

### 2) MAPPING THE SURFACE RESIDUAL FLOW TO DEPTH

Given the above estimate of $\Psi_{\text{res}}$ at the surface, how can we map it down to depth? Away from the effect of surface buoyancy fluxes (8) reduces to

$$J(\Psi_{\text{res}}, \overline{b}) = \kappa \frac{\partial^2 b}{\partial z^2}. \tag{12}$$

If we consider (12) as we travel down from the surface *along an isopycnal*, where $\overline{b}$ is constant, then we have

$$\frac{d\Psi_{\text{res}}}{ds} = \kappa \frac{\overline{b}_{zz}}{\sqrt{(\overline{b}_y)^2 + (\overline{b}_z)^2}}, \tag{13}$$

where $s$ is the distance traveled down along the isopycnal.[1]

This equation implies that below the mixed layer $\Psi_{\text{res}}$ changes on isopycnal surfaces because of small-scale diffusion. Given the residual circulation at the surface as an initial value, we can simply integrate (13) down along isopycnals to determine the complete structure of the residual circulation in the interior. The forcing on right-hand side of (13) is positive—the diffusion is positive and the stratification is stable. Therefore, as we move down along an isopycnal, the residual circulation increases—essentially generating an increase in the upward residual transport to balance the downward diffusion (see discussion in KJM). Alternatively, we can think of small-scale diffusion as increasing the buoyancy of deeper water, which then must move upward across isopycnals to maintain a steady stratification.

In Fig. 4, we plot the mean residual circulation versus depth and streamline for a vertical diffusivity $\kappa = 1.5 \times 10^{-5}\ \text{m}^2\ \text{s}^{-1}$. The cross-stream circulation of the ACC is dominated by two overturning cells. In the lower cell, deep water (neutral density approximately 27.7) is drawn poleward and upward, surfacing poleward of the ACC. It then travels equatorward along the surface toward the axis of the ACC where it subducts as AAIW (neutral density 27–27.4). In the upper cell, water of neutral density less than 27 surfaces equatorward of the ACC and is transported poleward to the center of the ACC where it subducts. In the region shown in Fig. 4, the lower cell comprises upwelling of 16.4 Sv of North Atlantic Deep Water (NADW) that is transformed in to AAIW while the upper cell represents the transformation of 14.3 Sv of SAMW into AAIW. Summing the two gives a net transport of 30.7 Sv of AAIW equatorward transport. The majority of the water transformation is due to surface buoyancy fluxes. For example, consider the flow in the mixed layer at the southern boundary of the ACC. Here the northward residual circulation of 13.2 Sv is being driven by a mass transformation of 15.4 Sv of denser water into lighter water due to air–sea fluxes offset by a transformation of 2.2 Sv of lighter water into dense water due to diffusion.

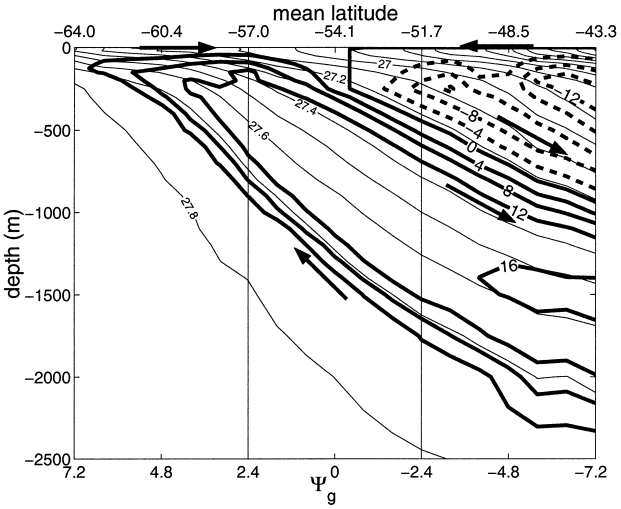


FIG. 4. The residual circulation streamfunction in Sverdrups versus depth and streamline: contour interval is 4 Sv with solid (dashed) contours indicating positive (negative) values. The arrows mark the direction of flow. The faint lines are contours of neutral density with a contour interval of 0.1.

It should be noted that the net cross-stream fluxes of buoyancy, heat, and salt calculated using our residual circulation are small. For example, there is a net equatorward heat flux of about 0.1 PW across the northern boundary of the ACC—this is the net flux in the upper 1500 m, the depth to which we can calculate the residual circulation at this latitude. For comparison the surface Ekman transport carries roughly 0.6 PW equatorward across the northern boundary of the ACC. Therefore, the eddies carry roughly 0.5 PW poleward, an estimate

[1] Equation (13) is derived by dividing (12) by

$$\sqrt{(\overline{b}_y)^2 + (\overline{b}_z)^2}$$

and using that

$$dy/ds = \overline{b}_z/\sqrt{(\overline{b}_y)^2 + (\overline{b}_z)^2} \quad \text{and} \quad dz/ds = -\overline{b}_y/\sqrt{\overline{b}_y^2 + \overline{b}_z^2}.$$

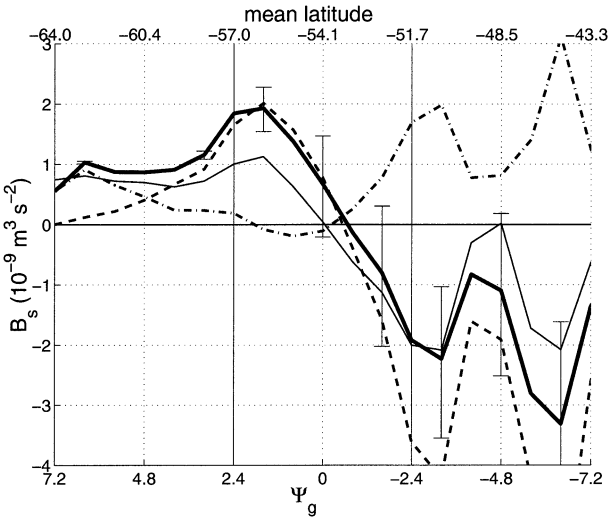


FIG. 5. The implied mean surface buoyancy fluxes using $\Psi_{res}$ computed from SOC winds (thick solid) and the portions of this flux due to heat (dashed) and salinity (dot–dash) fluxes. The thin solid line is the implied buoyancy flux using HR winds. The error bars are those associated with our estimate of eddy diffusivity.

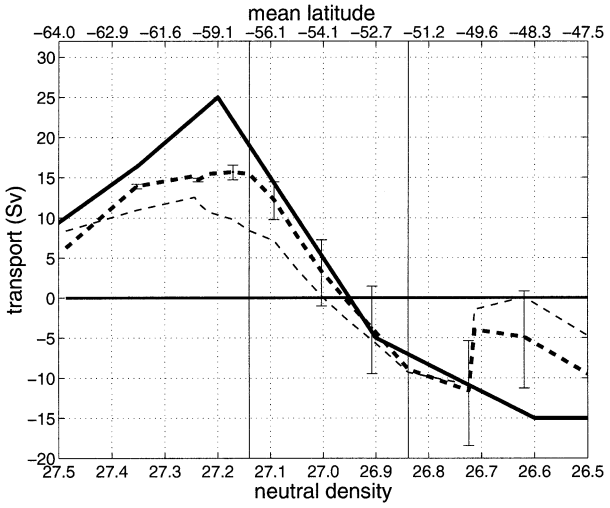


FIG. 6. The buoyancy-driven transport, $\Psi_B$, given by (14). The solid line is from Speer et al. (2000) and is calculated using observations of the air–sea fluxes. The dashes lines are our estimates calculated using the residual circulation, $\Psi_{res}$. The thick dashed line is our estimate based on SOC winds and the thin dashed line is based on HR winds. The error bars are those associated with the eddy diffusivity.

that sits within the range of previous ones—for example, 0.3 PW (Stammer 1998), 0.5 PW (de Szoeke and Levine 1981), 0.9 PW (Phillips and Rintoul 2000), and many more.

### *c. Implied buoyancy fluxes*

From (10) we can infer the air–sea buoyancy flux from our calculated residual circulation and the surface buoyancy gradient. We plot the inferred mean buoyancy flux in Fig. 5 as well as its component parts, the heat and salinity fluxes. The curve indicates a gain of buoyancy by the ocean at the poleward boundary and a loss of buoyancy at the equatorward boundary of our domain. The magnitude of the flux is plausible—the maximum heat gain corresponds to 12 W $m^{-2}$. Over the ACC, heat flux dominates. Poleward of the ACC, freshwater fluxes dominate heat fluxes to maintain a significant buoyancy gain. These freshwater fluxes are most likely to be due to a combination of precipitation and ice melt depending on the proximity to Antarctica. Equatorward of the ACC, both contributions are important but tend to offset one another in the buoyancy budget.

The pattern of heat flux is almost the exact opposite of what one might naively expect. The traditional picture has heat loss near the pole and heat gain in the subtropics. However, with few land masses in the Southern Hemisphere, air and sea temperatures are in rough equilibrium (Speer et al. 2000). The Polar Front separates the cold AASW from the warmer SAMW and the overlying atmosphere must have a similar front. Air–sea heat fluxes largely occur when perturbations to these fronts disturb the equilibrium between the ocean and atmosphere. If a cold atmospheric anomaly moves equatorward of the Polar Front, the ocean will lose heat to this anomaly. On the other hand, if a warm atmospheric anomaly moves poleward of the Polar Front, the ocean will gain heat from this anomaly. Thus, we have heat loss equatorward and gain poleward with the latitude of zero heat flux marking the Polar Front, as in Fig. 5 and the observations discussed in Speer et al. (2000).

If, however, it is assumed that ocean perturbations are more important in inducing air–sea fluxes (unlikely to be true except perhaps on the longest of timescales), the exact opposite is obtained: heat gain by the ocean on the equatorward flank and loss poleward of the Polar Front. Such is the case in most OGCMs that use restoring boundary conditions—in essence a fixed atmosphere—and may explain the discrepancy between observed patterns of heat flux and those derived from models.

The balance (10) can be rearranged to define a transport $\Psi_B$, given by

$$\Psi_B = \frac{B_s}{\overline{b}_y} = \Psi_{res} + \kappa \frac{\overline{b}_z}{\overline{b}_y}, \tag{14}$$

where $\Psi_B$ was the quantity computed by Speer et al. (2000) based on observations of $B_s$—they used COADS data and an inverse model to infer air–sea fluxes: $\Psi_{res}$ is the circulation computed here and the diffusive term can be computed from the hydrography using $\kappa = 1.5 \times 10^{-5}$ $m^2$ $s^{-1}$. Thus, (14) gives us two independent ways estimating $\Psi_B$. In Fig. 6, we plot $\Psi_B$ based on Fig. 3 of Speer et al. (2000) and based on our calculation of $\Psi_{res}$. It is clear that the two estimates have broad similarities and encouraging that two different ap-

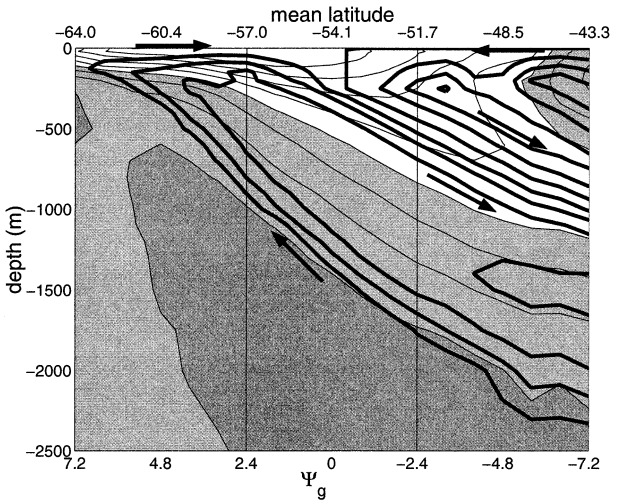


FIG. 7. The thin lines are contours of mean salinity. The region of no shading marks fresh AASW and AAIW, salinity <34.4 psu; the darkest shading marks salty NADW, salinity >34.7 psu. The dark solid lines are contours of the residual circulation with the arrows showing the direction of flow.

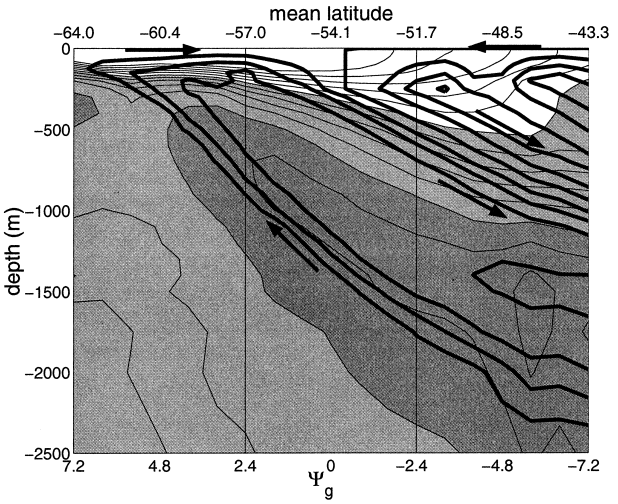


FIG. 8. The thin lines are contours of the mean dissolved oxygen. The region of no shading marks high-oxygen AASW and AAIW, dissolved oxygen >5.75 mL $L^{-1}$; the darkest shading marks low-oxygen NADW, dissolved oxygen <4.5 mL $L^{-1}$. The dark solid lines are contours of the residual circulation with the arrows showing the direction of flow.

proaches lead to a similar pattern and position of the convergence zone.

It should be noted that Speer et al. (2000) argued that eddies do not play an important role in the water transformation of the ACC. Our calculations support this conclusion at the poleward boundary of the ACC, where eddy fluxes are weak and to leading order surface fluxes balance Ekman transport. However, this is certainly not true on the equatorward flank of the ACC where the eddies are very strong and appear to balance the Ekman transport.

### *d. Tracer transport*

In this section, by making reference to the distribution of salinity and oxygen, we examine whether our calculated residual circulation is consistent with these tracer fields. We choose salinity and oxygen because climatological datasets are available from Levitus and Boyer (1994) and because their structure differs considerably from the buoyancy.

In Fig. 7 the salinity field is presented using a grayscale. The light region at the surface poleward of the ACC marks freshwater formed as ice melts. The signal of this freshwater is seen as a tongue of low salinity water that extends equatorward under the ACC. This tongue clearly marks the subduction of low salinity water to form AAIW. There is also evidence of high salinity NADW upwelling to the surface. Superimposed in the figure are the streamlines of the residual circulation with arrows indicating the direction of flow. They suggest that the freshwater formed by ice melt is advected equatorward and then subducted near the center of the ACC. The path of the flow suggested by the residual circulation agrees remarkably well with the observed salinity tongue. The upwelling tongue of NADW, however, appears to lie slightly deeper than the upwelling limb of our residual circulation. We believe this is clear evidence that the large-scale pattern of the residual circulation calculated here is plausible.

In Fig. 8, we superimpose the distribution of dissolved oxygen with the residual circulation. The oxygen distribution shows two striking features. First, the low temperature surface waters poleward of the ACC have a very high concentration of oxygen. This region of well-oxygenated water also extends equatorward as a tongue under the ACC, tagging AAIW as freshly ventilated water. Second, there is a tongue of low oxygen water extending poleward at greater depths and rising almost to the surface marking unventilated NADW.

Again the pattern of dissolved oxygen is in broad agreement with our pattern of residual circulation. Low oxygen waters are transported poleward at depth across the ACC, rising upward until they are brought to the surface poleward of the ACC. These waters are oxygenated as they return equatorward at the surface to be subducted near the axis of the ACC forming well-ventilated AAIW.

It has long been postulated that such overturning cell must exist in order to explain the observed water masses and the transformation of NADW to AAIW (see the discussions in Speer et al. 2000). We see here how this circulation pattern might come about and the importance of eddies in contributing to it. The fact that our inferred circulation agrees well qualitatively with the salinity and oxygen distributions adds credence to the methods used to infer it.

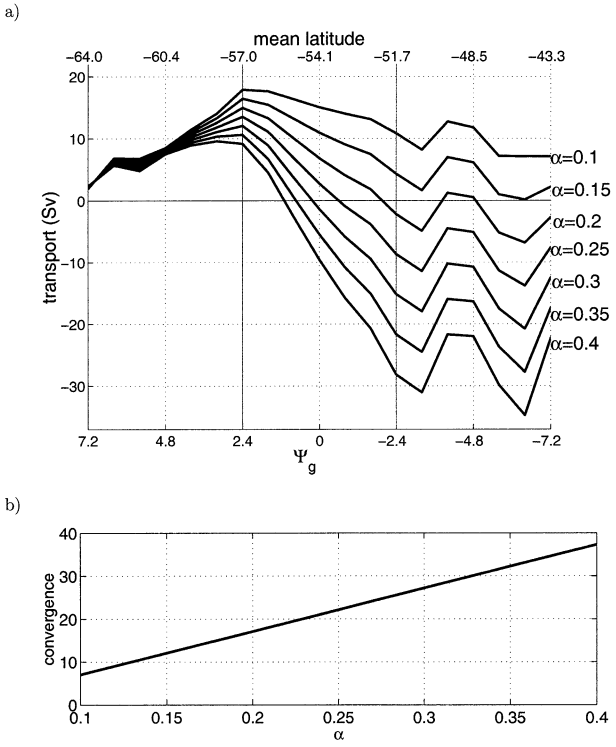


FIG. 9. (a) The residual circulation for different values of $\alpha$. (b) The net convergence into the ACC vs $\alpha$.

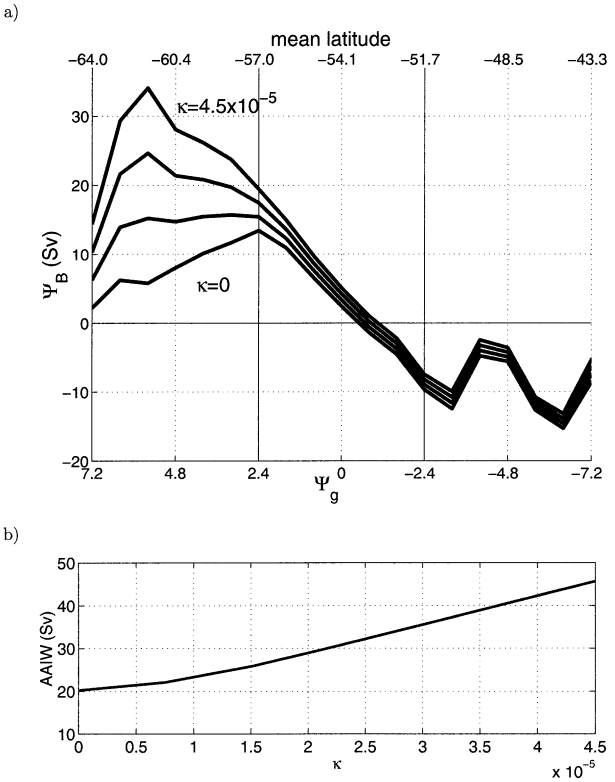


FIG. 10. (a) The buoyancy-driven transport, $\Psi_B$, as given in (14) for $\kappa = 0$, 1.5, 3, and 4.5 ($\times 10^{-5}$ m$^2$ s$^{-1}$). (b) The net flux of AAIW across the northern boundary of the ACC vs $\kappa$.

### e. Varying $\alpha$ and $\kappa$

The values chosen for the parameters $\alpha$ and $\kappa$ in the calculations, presented above, are somewhat constrained by observations and models, but are not known within a factor of 2 or so. We therefore briefly discuss how our results change if these values are altered. The scale factor $\alpha$ essentially changes the magnitude of the eddy flux and hence the magnitude of the transport associated with eddies. In Fig. 9a we plot the surface residual circulation for several values of $\alpha$. As $\alpha$ is varied, we see little change in the broad pattern of the residual circulation: there is always convergence of surface flow in to the axis of the ACC and hence a subduction zone. However, if the eddy contribution is reduced, we do not observe poleward flow on the equatorward flank of the ACC—and no associated region of buoyancy loss to the atmosphere. Instead we observe a weak equatorward flow there. In Fig. 9b we plot the convergence of flow into the ACC versus $\alpha$. This convergence, and hence the subduction of AAIW, varies linearly with $\alpha$ ranging from 7 to 37 Sv as $\alpha$ increases from 0.1 to 0.4. This increase in convergence results from the increased southward flow of SAMW driven by the stronger eddies.

We can also examine the effect of varying the vertical mixing in our calculations. In Fig. 10 we examine two results of varying the vertical diffusion $\kappa$. First, the mixed layer balance (10) stipulates that an increase in vertical diffusivity must be offset by an increase in surface fluxes to maintain the same residual circulation. Thus, as shown in Fig. 10a, varying the diffusivity changes the implied buoyancy-driven transport, see (14). Particularly, the positive buoyancy fluxes south of the ACC vary by a factor of 4 as we change from no vertical diffusion to a high diffusivity of $4.5 \times 10^{-5}$ m$^2$ s$^{-1}$. This is a result of the strong surface stratification south of the ACC. The buoyancy-driven transport can easily equal or exceed that calculated by Speer et al. (2000) in this region for reasonable values of diffusivity. It suggests that, if the diffusivities in this region are large, very large surface buoyancy fluxes (possibly due to ice melt at these high latitudes) could be balanced by a combination of Ekman transport and vertical diffusion.

Second, increasing vertical mixing requires an increase in the net overturning of the meridional cell and hence increases the estimate of production rates of AAIW. In Fig. 10b we plot the net flux of AAIW across the northern boundary of the ACC versus $\kappa$. We see the flux of AAIW increases linearly for larger values of $\kappa$, from 25 to 35 Sv as $\kappa$ increases from a moderate value of $1.5 \times 10^{-5}$ to $3 \times 10^{-5}$ m$^2$ s$^{-1}$. Obviously, mixing processes can play an important role in water transformation.

## 4. Conclusions

In this paper we have used hydrographic and altimetric data to infer the residual circulation of the ACC using residual-mean theory. On the equatorward flank of the ACC, the residual circulation is much smaller than the individual terms that make it up (see Fig. 3) demonstrating that a leading order balance between eddy transport and Ekman transport is observed—the vanishing of the Deacon cell documented in numerical simulations. In this limit, the input of momentum at the ocean surface by wind stress is balanced by its transfer vertically through the column to depth by interfacial eddy form stress (Johnson and Bryden 1989; Olbers 1998). However, on the poleward side of the ACC, the eddies appear to be much weaker and the leading order balance is between the surface buoyancy gain and equatorward Ekman flow, as suggested in Speer et al. (2000).

The residual circulation has a surface convergence into the ACC (the Antarctic convergence) implying a subduction of AAIW. The latitude at which the residual circulation changes sign at the surface also establishes the position of the Polar Front—the front between cold AASW and warm SAMW where subduction occurs. The position of the Polar Front agrees roughly with that found in Moore et al. (1999), although further comparison is required. In addition we have shown that our surface pattern of residual circulation implies a surface buoyancy flux whose variation is in plausible agreement with the observations. This pattern is not intuitively obvious, suggesting as it does that buoyancy is gained by the ocean on the poleward flank of the ACC and lost by the ocean equatorward of the ACC.

When the residual circulation is mapped to depth, the result is two counterrotating cells: a strong cell associated with the transformation of NADW to AAIW and a weaker cell associated with the transformation of SAMW to AAIW. Assuming a value of vertical diffusivity of $1.5 \times 10^{-5}$ m$^2$ s$^{-1}$, these cells are driven primarily by the surface buoyancy fluxes. The pattern of subduction near the center of the ACC agrees remarkably well with the tongues of low salinity, high oxygen water found in the hydrographic record. The pattern of circulation is robust to changes in the scale factor $\alpha$ and the vertical diffusivity, although the strength of the flow is sensitive to variations in these parameters. Further studies that examine the rate of formation of AAIW and the spreading of tracers are required to determine if the magnitude of the flow given here is reasonable.

One step in this direction is to compare our results with other studies such as that of Sloyan and Rintoul (2001) who use inverse models and estimates of observed buoyancy fluxes to infer water mass transformation rates. Their calculations also imply a strong buoyancy flux into the ocean near the southern boundary of the ACC, equivalent to 24 Sv of mass transformation, a value consistent with our results if the vertical diffusivity is high. But they suggest that it is almost entirely composed of freshwater fluxes due in large part to precipitation over the southern Indian and Pacific Oceans, in contrast to the earlier study of Speer et al. (2000). The differences in these calculations arise from differences in the averaging methods (B. Sloyan 2002, personal communication) and hints at the difficulty of calculating surface fluxes. Our calculated residual circulation combined with a strong surface temperature gradient imply a strong heat flux at the southern boundary of the ACC but do allow for large freshwater fluxes farther south. Sloyan and Rintoul (2001) also describe a meridional overturning cell that transforms deep water into AAIW, although there are quantitative differences between our estimates and theirs which have yet to be reconciled.

In addition to reaffirming the dynamical balance of the ACC, our work illustrates the usefulness of the diffusivity formula (4) developed by Holloway (1986) and Keffer and Holloway (1988). Combined with the findings of Kushner and Held (1998), our work suggests that further studies should take advantage of this formulation. An essential aspect is determination of the parameter $\alpha$ from observations and models. One could obtain a value for $\alpha$ by determining an independent estimate of where the residual circulation vanishes using, for example, the point where the observed buoyancy flux vanishes (see Speer et al. 2000) or the point where the potential vorticity gradient vanishes (see Marshall et al. 1993).

It is perhaps best to view our findings as an initial foray into using observations to examine the residual circulation of the ACC. Given the limits of the data available, we find our results extremely encouraging. As observational databases improve, we expect that a considerably more accurate picture will emerge. As well, the ACC, the air–sea forcing driving it, and the properties of the water around it can vary substantially along its path (see Sloyan and Rintoul 2001). Our approach has examined the streamline average of the ACC, and it is worthwhile to consider how to extend our results to examine regional balances.

*Acknowledgments.* We thank the Physical Oceanography Division of the National Science Foundation, whose support made this study possible.

## APPENDIX

### Testing the Keffer and Holloway Eddy Diffusivity

We test relation (4), discused in section 2, that states $K$ is proportional to the height variance using the reference numerical experiment of KJM. In Fig. A1, we plot the diagnosed eddy diffusivity and the formula given in (4) with $\alpha = 0.26$ versus the cross-stream coordinate. Clearly the formula is capturing the cross-stream variation of the real eddy diffusivity.

The use of the KJM experiments to evaluate a $K$

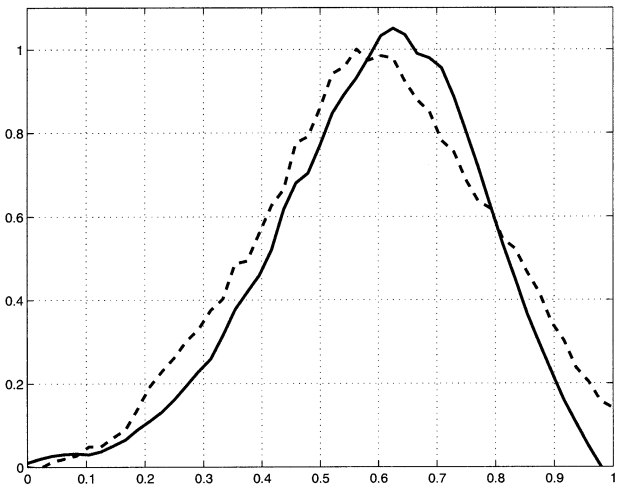


FIG. A1. The eddy buoyancy flux vs cross-stream coordinate as diagnosed from the numerical simulation of KJM (dashed) and as calculated using (4) with $\alpha = 0.26$ (solid). Magnitudes have been normalized by the maximum of the diagnosed flux.

appropriate to the ACC is perhaps limited. The symmetry of the domain and forcing constraints limit the spatial variance of the mean eddy fluxes. It is possible that the experiments are over damped in the surface layers, decreasing the calculated value of $\alpha$ (see Kushner and Held 1998). In addition, the lack of topography changes the structure of the eddies, eliminating the standing waves that form downstream of topographic features. As seen in mooring data (see Phillips and Rintoul 2000), such large-scale, slowly evolving waves can greatly affect the eddy fluxes. Thus, even though we use the value of $\alpha$ determined by the numerical experiments in the body of the paper, further examination of eddy-resolving models with topography is required.

## REFERENCES


Andrews, D. G., and M. E. McIntyre, 1976: Planetary waves in horizontal and vertical shear: The generalized Eliassen–Palm relations and the mean zonal acceleration. *J. Atmos. Sci.,* **33,** 2031–2048.

——, J. Holton, and C. Leovy, 1987: *Middle Atmosphere Dynamics.* Academic Press, 489 pp.

Bryden, H. L., and R. A. Heath, 1985: Energetic eddies at the northern edge of the Antarctic Circumpolar Current. *Progress in Oceanography,* Vol. 14, Pergamon, 65–87.

Danabasoglu, G., J. C. McWilliams, and P. Gent, 1994: The role of mesoscale tracer transport in the global ocean circulation. *Science,* **264,** 1123–1126.

Deacon, G., 1984: *The Antarctic Circumpolar Current.* Cambridge University Press, 180 pp.

de Szoeke, R. A., and M. D. Levine, 1981: The advective flux of heat by mean geostrophic motions in the Southern Oceans. *Deep-Sea Res.,* **28,** 1057–1085.

Döös, K., and D. Webb, 1994: The Deacon Cell and other meridional cells of the Southern Ocean. *J. Phys. Oceanogr.,* **24,** 429–442.

Gent, P. R., W. G. Large, and F. O. Bryan, 2001: What sets the mean transport through the Drake Passage? *J. Geophys. Res.,* **106,** 2693–2712.

Gill, A. E., 1982: *Atmosphere–Ocean Dynamics.* Academic Press, 662 pp.

Gille, S. T., 1997: The Southern Ocean momentum balance: Evidence for topographic effects from numerical model output and altimeter data. *J. Phys. Oceanogr.,* **27,** 2219–2231.

Gnanadesikan, A., 1999: A simple predictive model for the structure of the oceanic pycnocline. *Science,* **283,** 2077–2079.

——, and R. W. Hallberg, 2000: On the relationship of the Circumpolar Current to Southern Ocean winds in course-resolution ocean models. *J. Phys. Oceanogr.,* **30,** 2013–2034.

Held, I. M., and T. Schneider, 1999: The surface branch of the zonally averaged mass transport circulation in the troposphere. *J. Atmos. Sci.,* **56,** 1688–1697.

Hellerman, S., and M. Rosenstein, 1983: Normal monthly wind stress over the worlds ocean with error estimates. *J. Phys. Oceanogr.,* **13,** 1093–1104.

Holloway, G., 1986: Estimation of oceanic eddy transports from satellite altimetry. *Nature,* **323,** 243–244.

Ivchenko, V. O., K. J. Richards, and D. P. Stevens, 1996: The dynamics of the Antarctic Circumpolar Current. *J. Phys. Oceanogr.,* **26,** 753–774.

Johnson, G. C., and H. L. Bryden, 1989: On the size of the Antarctic Circumpolar Current. *Deep-Sea Res.,* **36,** 39–53.

Josey, S. A., E. C. Kent, and P. K. Taylor, 1998: The Southampton Oceanography Centre (SOC) Ocean–Atmosphere Heat, Momentum and Freshwater Flux Atlas. Southampton Oceanography Centre Rep. 6, Southampton, United Kingdom, 30 pp.

Karsten, R. H., and J. Marshall, 2002: On the vertical stratification of the ACC. *Dyn. Atmos. Oceans,* in press.

——, H. Jones, and J. Marshall, 2002: The role of eddy transfer in setting the stratification and transport of a Circumpolar Current. *J. Phys. Oceanogr.,* **32,** 39–54.

Keffer, T., and G. Holloway, 1988: Estimating Southern Ocean eddy flux of heat and salt from satellite altimetry. *Nature,* **332,** 624–626.

Killworth, P. D., 1992: An equivalent-barotropic mode in the Fine Resolution Antarctic Model. *J. Phys. Oceanogr.,* **22,** 1379–1387.

Kushner, P. J., and I. M. Held, 1998: A test, using atmospheric data of a method for estimating oceanic eddy diffusivity. *Geophys. Res. Lett.,* **25,** 4213–4216.

Levitus, S., and T. Boyer, 1994: *Temperature,* Vol. 4, *World Ocean Atlas 1994,* NOAA Atlas NESDIS 4, 117 pp.

Marsh, R., A. J. G. Nurser, A. P. Megann, and A. L. New, 2000: Water mass transformation in the Southern Ocean of a global isopycnal coordinate GCM. *J. Phys. Oceanogr.,* **30,** 1013–1045.

Marshall, D., 1995: Topographic steering of the Antarctic Circumpolar Current. *J. Phys. Oceanogr.,* **25,** 1636–1650.

——, 1997: Subduction of water masses in an eddying ocean. *J. Mar. Res.,* **55,** 201–222.

Marshall, J., and G. Shutts, 1981: A note on rotational and divergent eddy fluxes. *J. Phys. Oceanogr.,* **11,** 1677–1680.

——, D. Olbers, H. Ross, and D. Wolf-Gladrow, 1993: Potential vorticity constraints on the dynamics and hydrography of the Southern Ocean. *J. Phys. Oceanogr.,* **23,** 465–487.

——, H. Jones, R. Karsten, and R. Wardle, 2002: Can eddies set ocean stratification? *J. Phys. Oceanogr.,* **32,** 26–38.

Moore, J. K., M. R. Abbott, and J. G. Richman, 1999: Location and dynamics of the Antarctic Polar front from satellite sea surface temperature data. *J. Geophys. Res.,* **104,** 3059–3073.

Munk, W. H., and E. Palmén, 1951: Note on the dynamics of the Antarctic Circumpolar Current. *Tellus,* **3,** 53–55.

Nowlin, W. D., Jr., and J. M. Klink, 1986: The physics of the Antarctic Circumpolar Current. *Rev. Geophys.,* **24,** 469–491.

Olbers, D., 1998: Comments on ''On the obscurantist physics of 'form drag' in theorizing about the Circumpolar Current.'' *J. Phys. Oceanogr.,* **28,** 1647–1654.

——, and V. O. Ivchenko, 2001: On the meridional circulation and balance of momentum in the Southern Ocean of POP. *Ocean Dyn.,* **52,** 79–93.

Orsi, A. H., T. Whitworth III, and W. D. Nowlin Jr., 1995: On the

meridional extent and fronts of the Antarctic Circumpolar Current. *Deep-Sea Res.*, **42A,** 641–673.

Phillips, H. E., and S. R. Rintoul, 2000: Eddy variability and energetics from direct current measurements in the Antarctic Circumpolar Current south of Australia. *J. Phys. Oceanogr.,* **30,** 3050–3076.

Rintoul, S., C. Hughes, and D. Olbers, 2001: The Antarctic Circumpolar Current System. *Ocean Circulation and Climate,* G. Siedler et al., Eds., International Geophysics Series, Vol. 77, Academic Press, 271–302.

Sloyan, B., and S. R. Rintoul, 2001: Circulation, renewal and modification of Antarctic mode water and intermediate water. *J. Phys. Oceanogr.,* **31,** 1005–1030.

Speer, K., S. R. Rintoul, and B. Sloyan, 2000: The diabatic Deacon cell. *J. Phys. Oceanogr.,* **30,** 3212–3222.

Stammer, D., 1998: On eddy characteristics, eddy transports, and mean flow properties. *J. Phys. Oceanogr.,* **28,** 727–739.

Toggweiler, J. R., and B. Samuels, 1998: On the ocean's large-scale circulation in the limit of no vertical mixing. *J. Phys. Oceanogr.,* **28,** 1832–1852.

Visbeck, M., J. Marshall, T. Haine, and M. Spall, 1997: Specification of eddy transfer coefficients in coarse-resolution ocean circulation models. *J. Phys. Oceanogr.,* **27,** 381–402.